

Supporting Information

Three-Dimensional Conducting Oxides Nanoarchitectures: Morphology-Controllable Synthesis, Characterization, and Applications in Lithium-Ion Batteries

Fa-Qian Liu,^a Huiming Wu,^b Tao Li,^c Lauren R. Grabstanowicz,^a Kahlil Amine,^b and Tao Xu^{*a}

^aDepartment of Chemistry and Biochemistry, Northern Illinois University, DeKalb, IL
60115, USA, ^bChemical Science and Engineering, Argonne National Laboratory,
Argonne, IL 60439, USA, ^cAdvanced Photon Source, Argonne National Laboratory,
Argonne, IL 60439, USA

* Address correspondence to txu@niu.edu

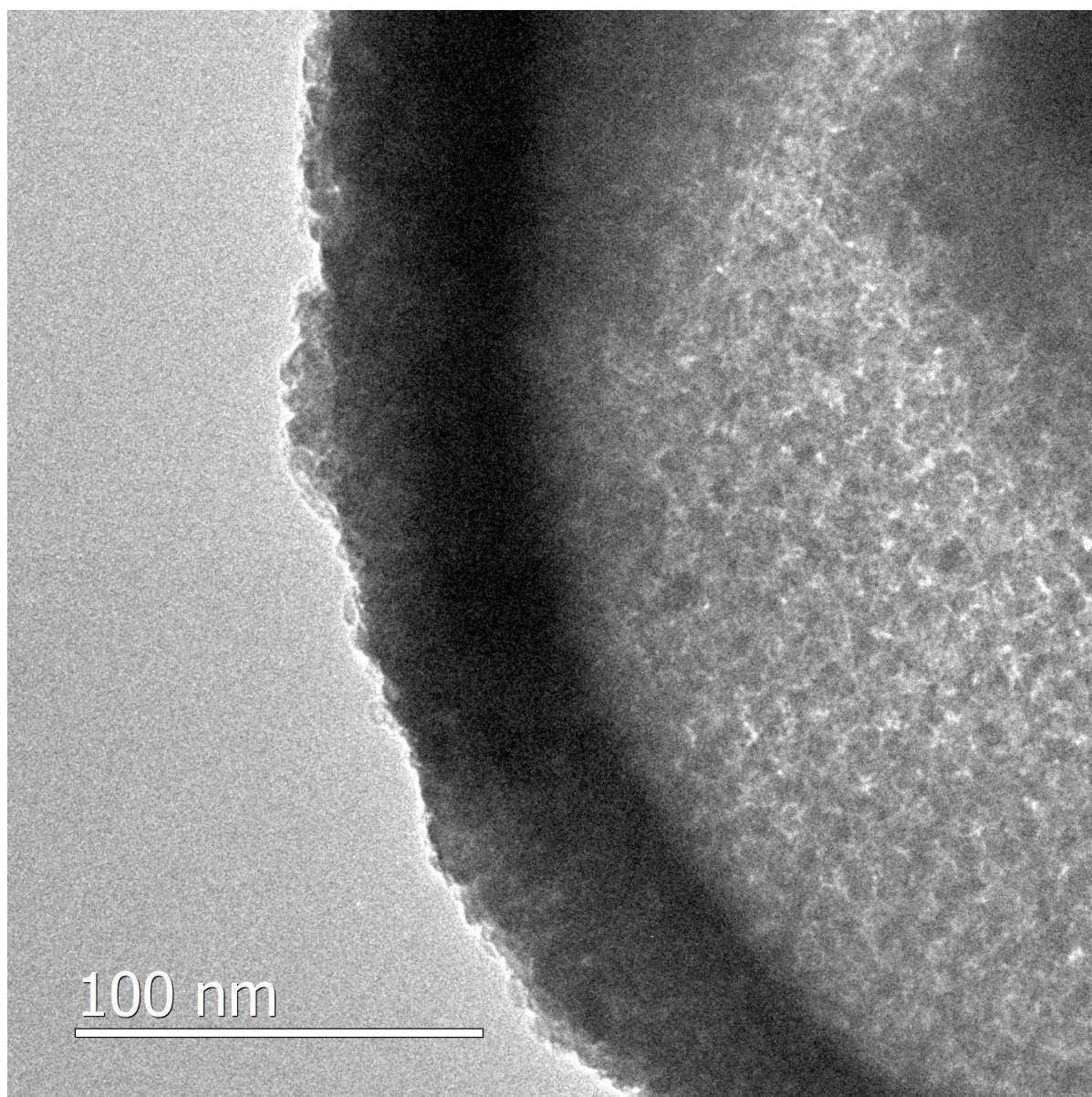


Fig. S1 TEM image of hollow nanobeads prepared from 526 nm sulfonated PS beads with higher concentration of precursors.

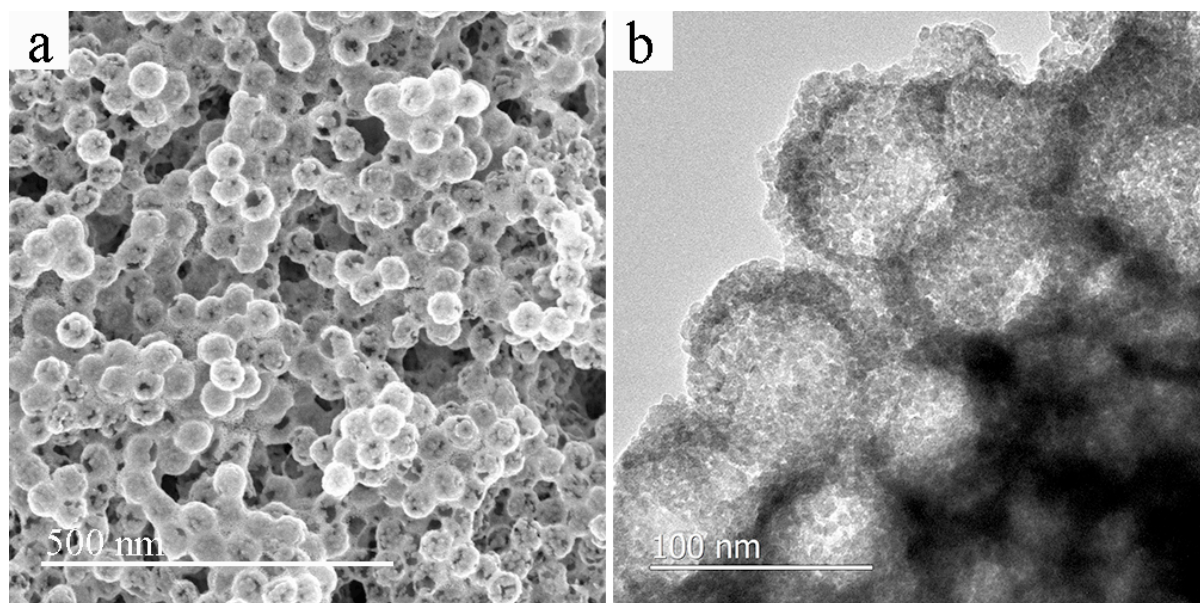


Fig. S2 SEM (a) and TEM (b) images of monodispersed hollow nanobeads prepared from 85 nm carboxylated PS spheres



Fig. S3 Cross-sectional SEM picture of a high-quality 3-D nanoporous FTO film as thick as 50 μm on the FTO glass, indicating the uniform and interconnecting 3-D nanoporous structure.

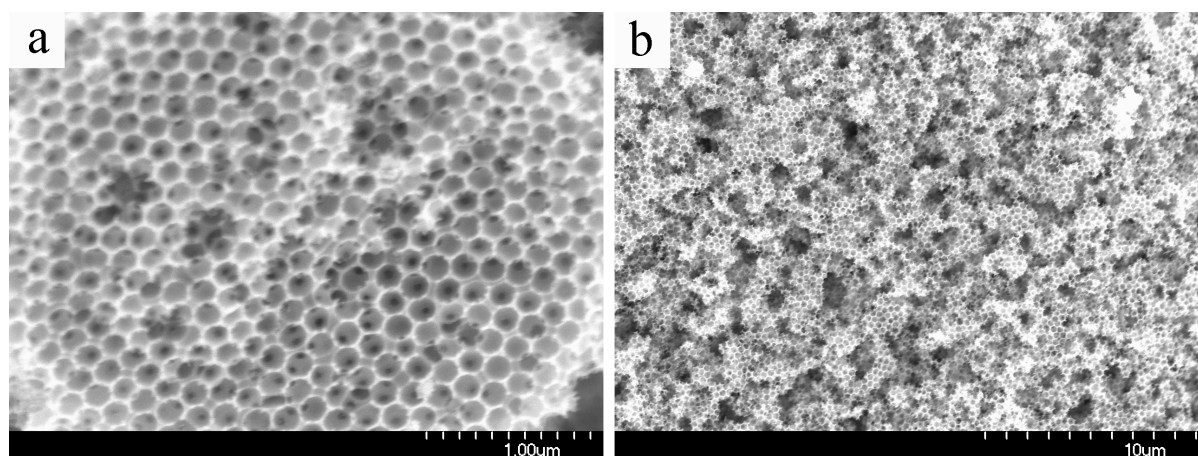


Fig. S4 SEM images of nanoporous structure prepared from 194 nm sulfonated PS beads (a) and 85 nm carboxylated PS beads (b).

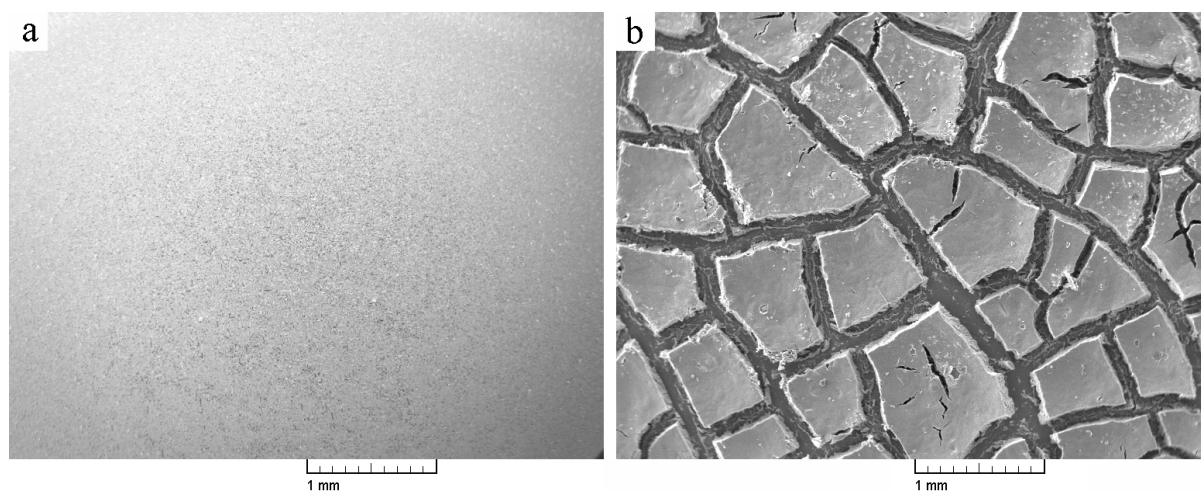


Fig. S5 (a) Large scale SEM image of FTO hollow nanobeads film prepared from 526 nm sulfonated PS beads, showing nearly crack-free; (b) Large scale SEM image of FTO hollow nanobeads film prepared from 526 nm pure PS beads, showing significant cracking.

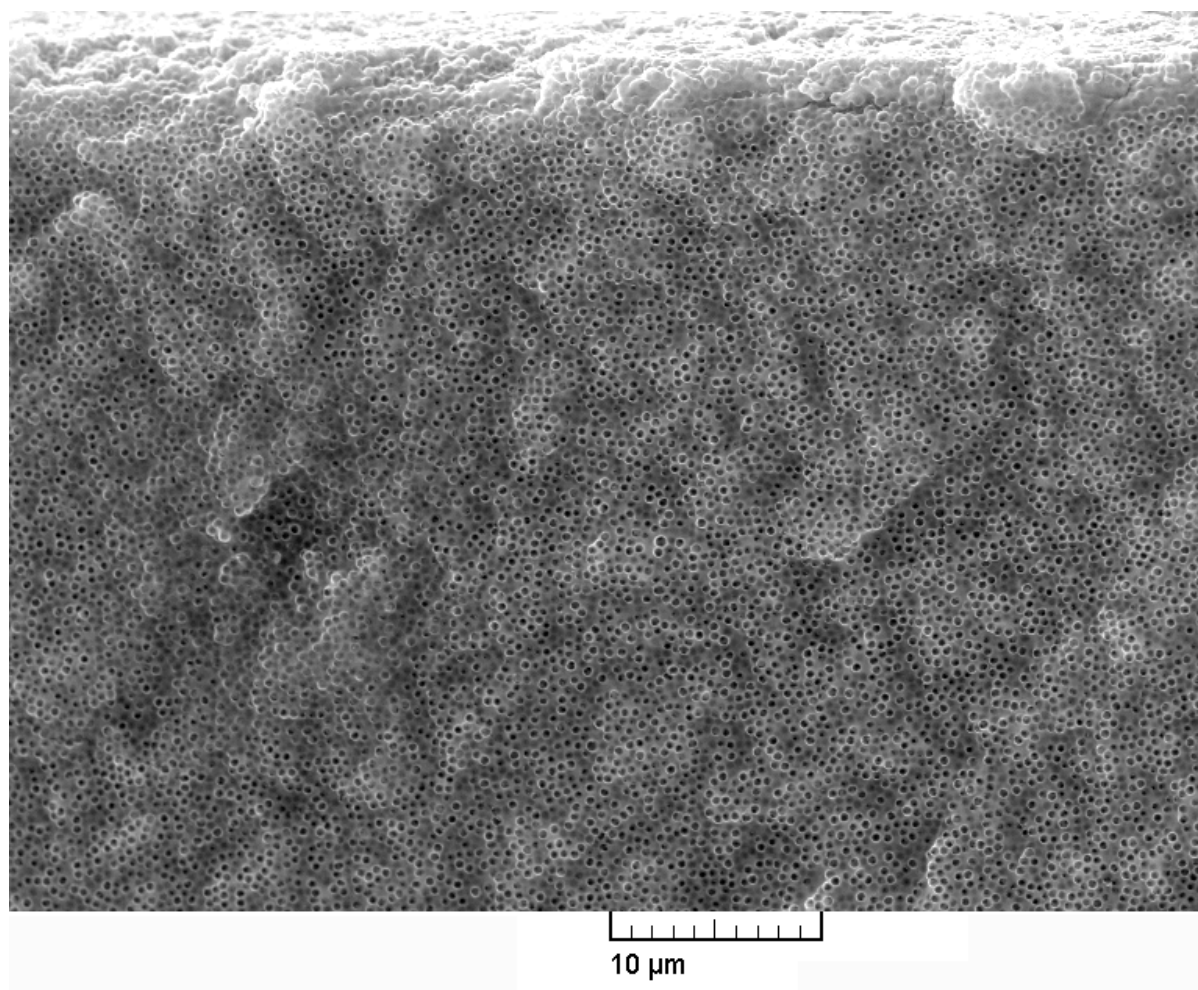


Fig. S6 Cross-sectional SEM image of a high-quality 3-D nanoporous film as thick as 50 μm on a FTO glass using a more concentrated FTO precursory solution (1.7 times greater than the one in the paper). 526 nm sulfonated PS beads were used as the template.

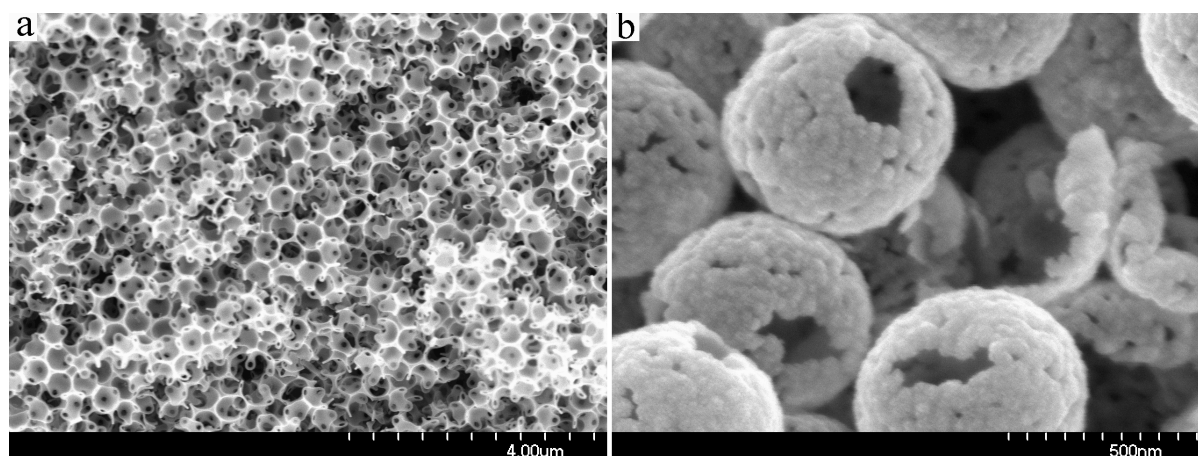


Fig. S7 (a) A typical SEM image of 3-D nanoporous FTO structure prepared by using SnCl_2 as precursor (route 1) but adding HNO_3 to neutralize the surface negative charge of 526 nm sulfonated PS beads. The increased acidity changed the morphology of the final nanostructure from FTO nanobeads to sponge-like nonporous FTO. (b) After tuning the pH of the above precursory solution up to 2 by addition of $\text{NH}_3 \cdot \text{H}_2\text{O}$, the SEM image shows the morphology of the final nanostructure as FTO nanobeads.

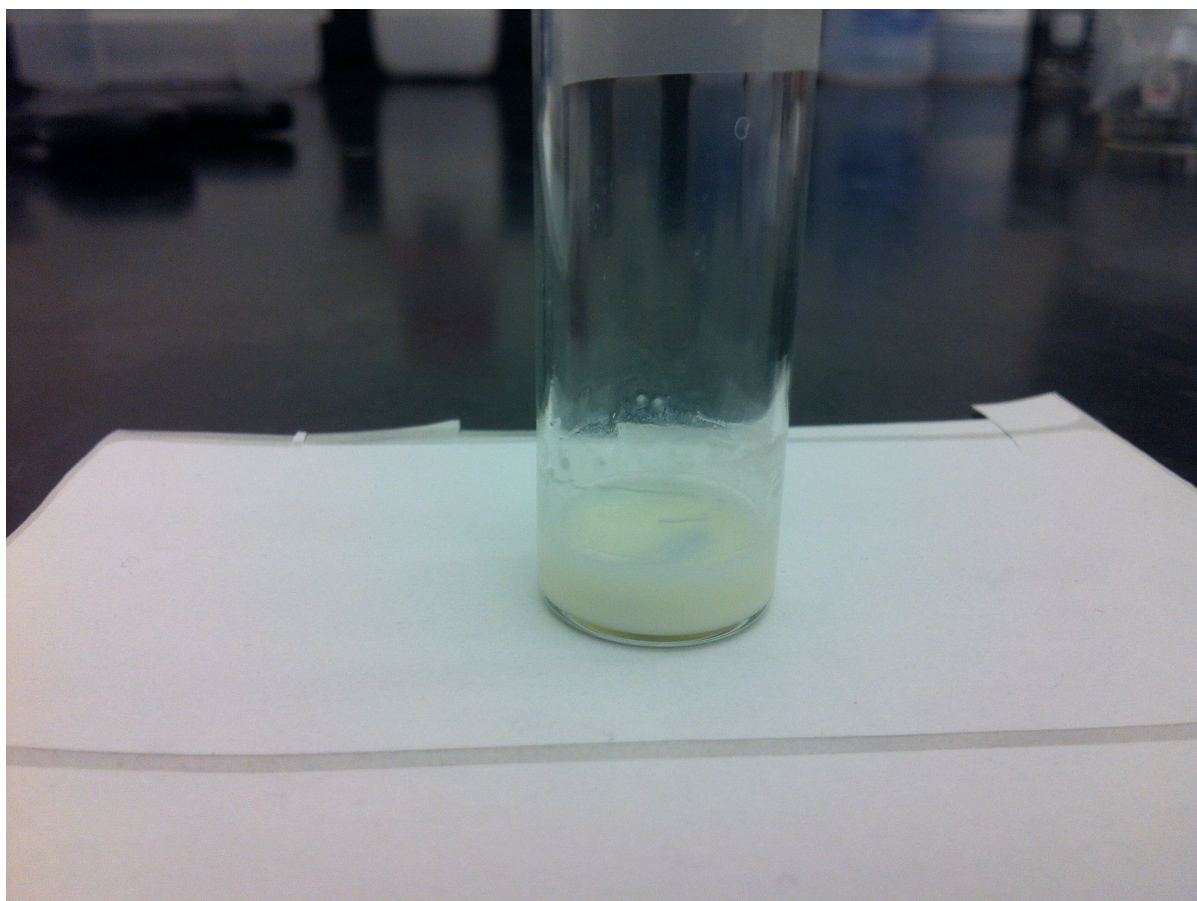


Fig. S8 The gel prepared via route 1 turns yellowish after oxidation in the air for over 72 hours. The starting precursor was $\text{SnCl}_2 \cdot 2\text{H}_2\text{O} + \text{NH}_4\text{F}$.

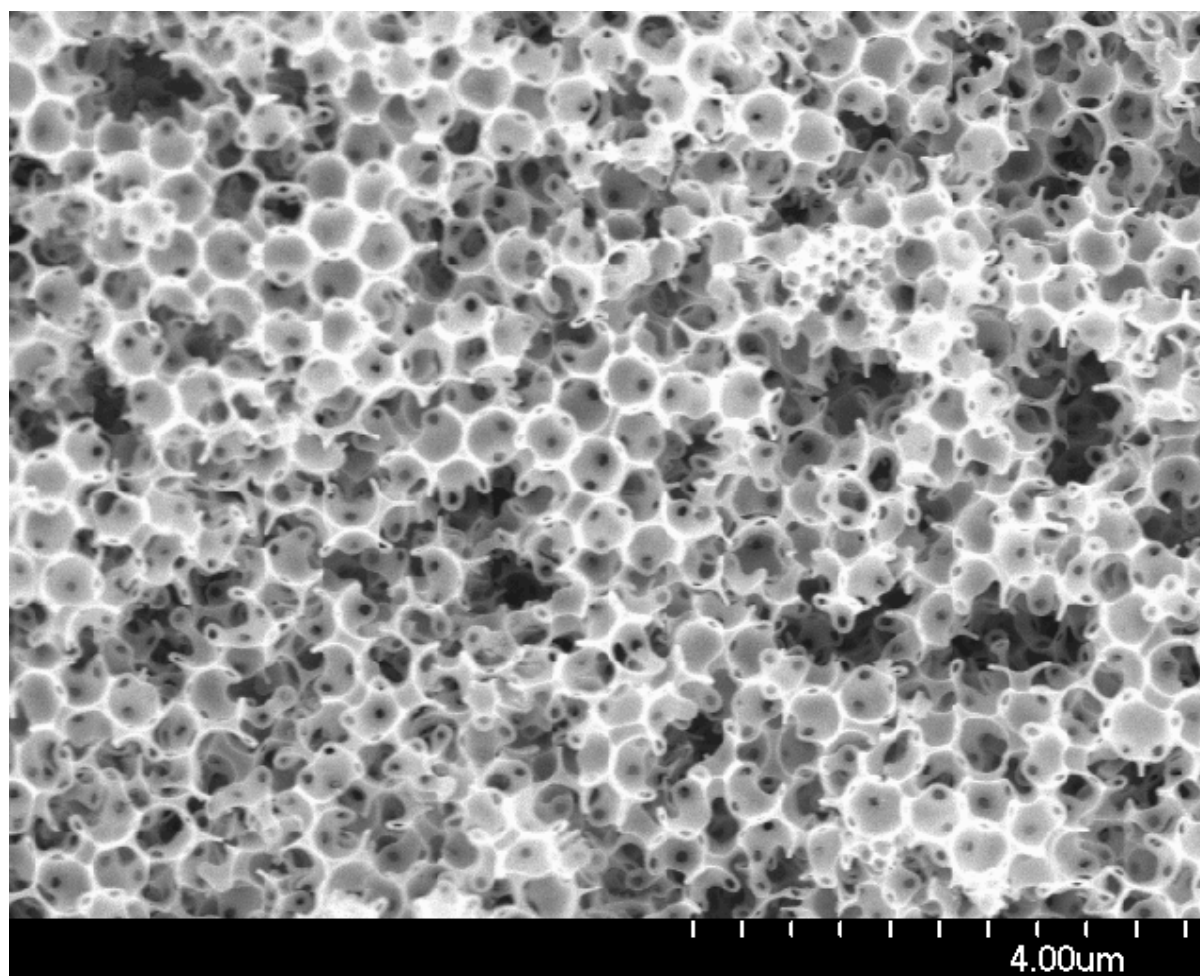


Fig. S9 SEM image of the 3-D nanoporous FTO structure prepared via route 1 by oxidizing the SnCl_2 precursory solution in the air for over 72 hours.

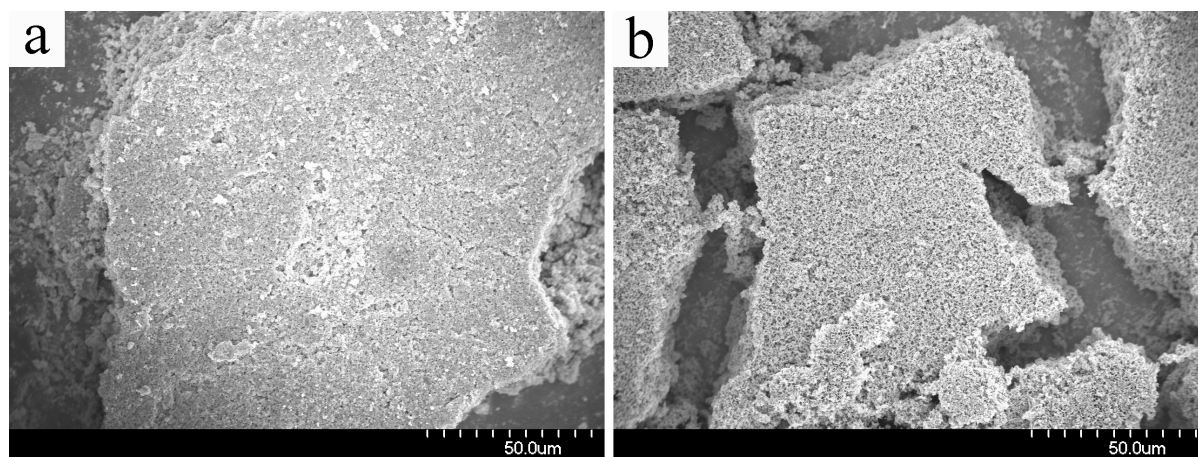


Fig. S10 The big cracks generated for the preparation of FHNB 526 (a) and NPF 526 (b) when the heating rate was set to 5 °C/min from 80-120 °C (route 1).

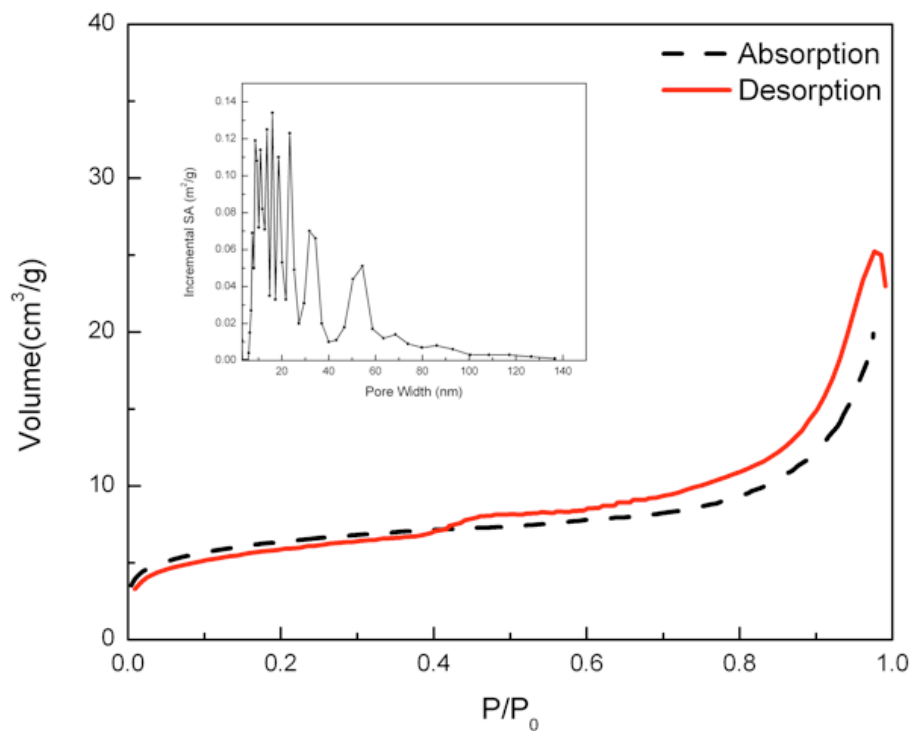


Fig. S11 Nitrogen adsorption/desorption isotherm of FHNB 526. The pore size distribution plot (inset) was calculated by original density functional theory.

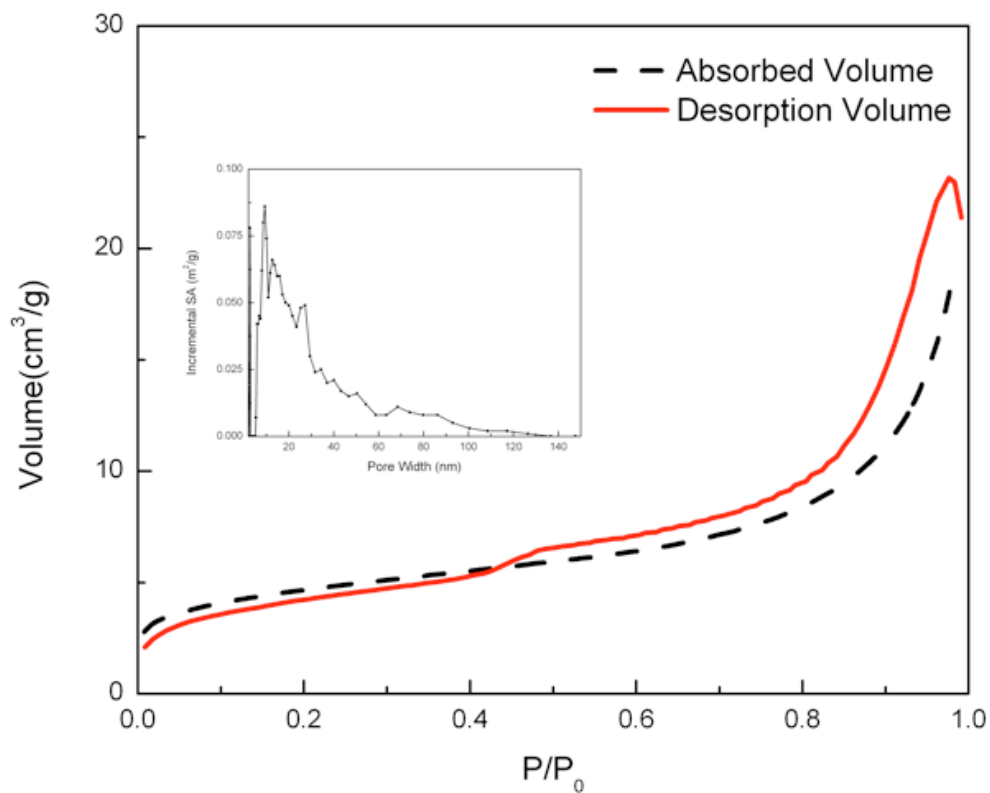


Fig. S12 Nitrogen adsorption/desorption isotherm of FHNB 85. The pore size distribution plot (inset) was calculated by original density functional theory.

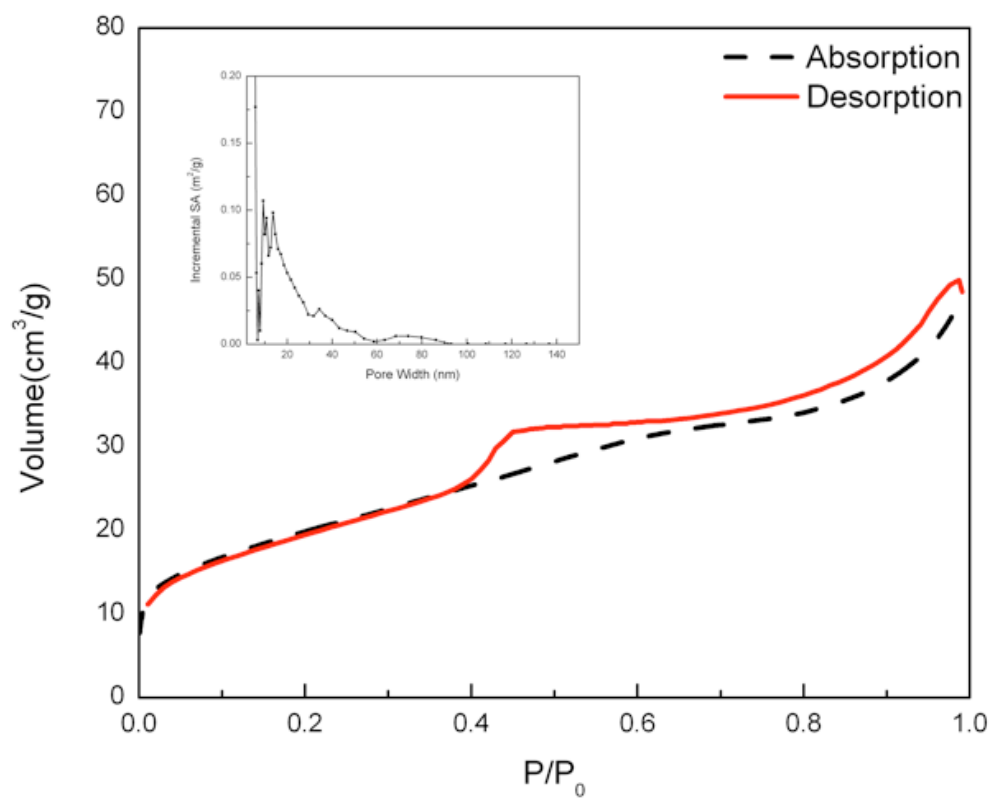


Fig. S13 Nitrogen adsorption/desorption isotherm of NPF 526. The pore size distribution plot (inset) was calculated by original density functional theory.

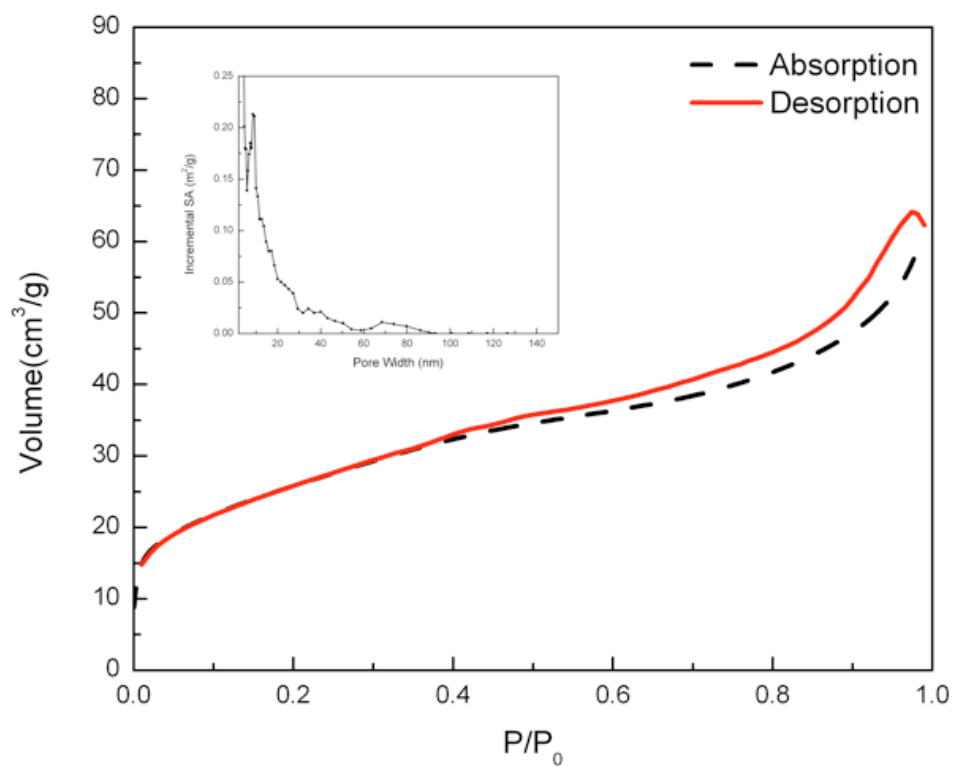


Fig. S14 Nitrogen adsorption/desorption isotherm of NPF 194. The pore size distribution plot (inset) was calculated by original density functional theory.

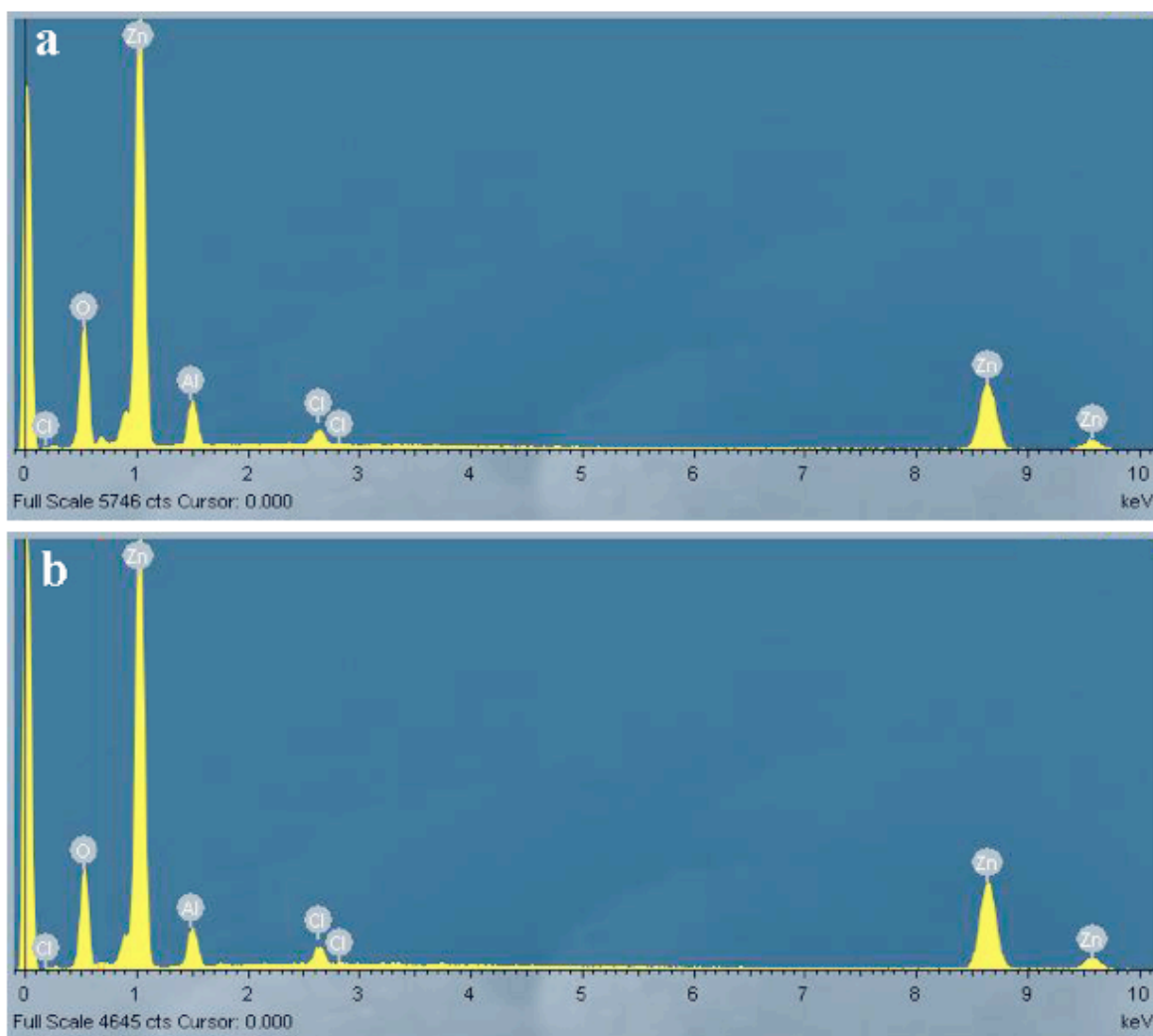


Fig. S15 The EDS profiles of (a) the synthesized AZO hollow spheres and (b) the porous AZO.